

Linear-Scaling Quantum Circuits for Computational Chemistry

Ilias Magoulas* and Francesco A. Evangelista*

*Department of Chemistry and Cherry Emerson Center for Scientific Computation, Emory
University, Atlanta, Georgia 30322, USA*

E-mail: ilias.magoulas@emory.edu; francesco.evangelista@emory.edu

Abstract

We have recently constructed compact, CNOT-efficient, quantum circuits for fermionic and qubit excitations of arbitrary many-body rank [I. Magoulas and F.A. Evangelista, *J. Chem. Theory Comput.* **19**, 822 (2023)]. Here, we present approximations to these circuits that substantially reduce the CNOT counts even further. Our preliminary numerical data, using the selected projective quantum eigensolver approach, demonstrate that there is practically no loss of accuracy in the energies compared to the parent implementation while the ensuing symmetry breaking is essentially negligible.

Chemistry has been identified as one of the first potential killer applications for quantum computing.¹ This is due to the fact that a quantum device can simulate a chemical problem with a number of computer elements (qubits) that scales, in principle, linearly rather than exponentially with system size. Even if an exponential advantage cannot be achieved for every chemical problem of interest,² any form of polynomial speed up could potentially bring classically intractable applications within computational reach.

Several low-depth hybrid quantum–classical approaches have been proposed that are suitable for current noisy intermediate-scale quantum hardware. In general, they can be

divided into two broad categories. The first family contains algorithms that rely on an ansatz, such as the variational (VQE),³⁻⁷ contracted,⁸ and projective⁹ (PQE) quantum eigensolvers, while the second is comprised of ansatz-independent schemes, including quantum imaginary time evolution^{10,11} and quantum subspace diagonalization methods.^{10,12-15}

Focusing on ansatz-dependent techniques that interest us more for the purposes of this work, the trial state is expressed in terms of a unitary parameterization, i.e.,

$$|\tilde{\Psi}(\mathbf{t})\rangle = U(\mathbf{t}) |\Phi\rangle, \quad (1)$$

where \mathbf{t} denotes a set of parameters and $|\Phi\rangle$ is a reference state that can be easily prepared on the quantum device, usually the Hartree-Fock Slater determinant. Chemically inspired ansätze are almost invariably based on the unitary extension¹⁶⁻²⁸ of coupled-cluster theory²⁹⁻³⁴ (UCC). In general, a factorized form of the UCC unitary is adopted,

$$U(\mathbf{t}) = \prod_{\mu} e^{t_{\mu} \kappa_{\mu}}, \quad (2)$$

also known as disentangled UCC,³⁵ that can be readily implemented on a quantum device. The κ_{μ} symbols appearing in eq (2) represent generic fermionic, anti-Hermitian, particle-hole excitation operators. For an n -tuple excitation, they are defined as

$$\kappa_{\mu} \equiv \kappa_{i_1 \dots i_n}^{a_1 \dots a_n} = a^{a_1} \dots a^{a_n} a_{i_n} \dots a_{i_1} - a^{i_1} \dots a^{i_n} a_{a_n} \dots a_{a_1}, \quad (3)$$

where a_p ($a^p \equiv a_p^{\dagger}$) is the second-quantized annihilation (creation) operator acting on spinorbital ϕ_p and indices i_1, i_2, \dots or i, j, \dots (a_1, a_2, \dots or a, b, \dots) label spinorbitals occupied (unoccupied) in $|\Phi\rangle$. An alternative strategy that leads to more efficient quantum circuits is to replace the fermionic anti-Hermitian operators by their qubit counterparts, defined as

$$Q_{i_1 \dots i_n}^{a_1 \dots a_n} = Q^{a_1} \dots Q^{a_n} Q_{i_n} \dots Q_{i_1} - Q^{i_1} \dots Q^{i_n} Q_{a_n} \dots Q_{a_1}, \quad (4)$$

with Q_p ($Q^p \equiv Q_p^\dagger$) denoting the qubit annihilation (creation) operator acting on the p^{th} qubit. However, in doing so, one may potentially sacrifice the proper sign structure of the resulting state,^{36–41} since qubit excitations neglect the fermionic sign. Designing efficient, i.e., low-depth and noise-resilient, quantum circuits representing fermionic and qubit excitations is crucial for the success of ansatz-dependent algorithms on current noisy quantum hardware.

Inspired by the work of Yordanov et al.,^{36,37} we have recently introduced compact fermionic (FEB) and qubit-excitation-based (QEB) quantum circuits that efficiently implement excitations of arbitrary many-body rank⁴¹ (see, also, ref 42 for an alternative CNOT-efficient approach that requires ancilla qubits). While the FEB/QEB quantum circuits are equivalent to their conventional analogs, i.e., there is no loss of accuracy in the simulations, they significantly reduce the numbers of single-qubit and, more importantly, CNOT gates (recall that experimental realizations of two-qubit gates, such as CNOT, tend to have errors that are about 10 times larger than those of the single-qubit ones⁴³). For example, the standard quantum circuit implementing a sextuple qubit excitation requires more than 45,000 CNOT gates while its QEB counterpart needs only about 2,000. Despite the drastic reduction in the CNOT count afforded by the FEB and QEB quantum circuits, their number continues to scale exponentially with the operator many-body rank. Consequently, quantum algorithms based on a full FEB/QEB operator pool will typically generate circuits with unfavorable CNOT counts when compared to approaches relying on pools containing lower-rank excitation operators, such as singles and doubles or their generalized extension.^{44,45}

As elaborated on in our earlier study,⁴¹ the multi-qubit-controlled R_y gate is the dominant source of CNOTs in the FEB/QEB quantum circuits. In that work, we relied on an ancilla-free implementation of that gate that requires 2^{2n-1} CNOTs, where n is the many-body rank of the given excitation operator. Adopting more efficient implementations of the multiply controlled R_y gate can significantly reduce the CNOT requirements. For example, the approach advocated in ref 46 results in the linear-scaling CNOT count of $12n - 14$, but requires $\lceil (2n - 3)/2 \rceil$ ancilla qubits, where $\lceil x \rceil$ denotes the ceiling of x . Recently, ancilla-

free, CNOT-efficient implementations of multiply controlled gates have been proposed. Of particular interest are the ones introduced in refs 47 and 48, which decompose the multi-qubit-controlled R_y gate into circuits containing $16n^2 - 24n + 10$ and, at most, $32n - 40$ CNOTs, respectively. All of these state-of-the-art decompositions generate FEB/QEB quantum circuits with significantly less CNOT gates compared to those reported in our earlier study, especially so as the many-body rank increases. Nevertheless, they either require ancilla qubits, have a $\mathcal{O}(n^2)$ scaling, or have large prefactors in the resulting CNOT counts.

In our efforts to design CNOT-frugal FEB/QEB quantum circuits, we opted for a different strategy. In this letter, we consider approximate implementations of the multi-qubit-controlled R_y gate in which the number of control qubits is reduced. Since the resulting circuits are not equivalent to their parent FEB/QEB counterparts, some loss of accuracy in the computed energies is anticipated. Furthermore, as shown analytically in the Supporting Information, the removal of control qubits leads to the breaking of the particle number (N) and total spin projection (S_z) symmetries, while spatial symmetry is still preserved. To demonstrate this effect, we performed single-point, VQE UCC with doubles (UCCD) simulations using the full QEB circuits and three approximations, the numerical results of which are depicted in Figure 1. In these illustrative calculations, we focused on the H_6 linear chain, as described by the STO-6G minimum basis.⁴⁹ The geometry that we selected was characterized by the distance between neighboring hydrogen atoms (R_{H-H}) of 2.0 Å, the largest H–H separation considered in our earlier study.⁴¹ As shown in Figure 1, the removal of controls from the multi-qubit-controlled R_y gate leads to a ‘leaking’ of the wavefunction into other symmetry sectors of the Fock space. Specifically, we observe contaminants with eigenvalues of N and S_z that differ by ± 2 and ± 4 for N , and ± 1 and ± 2 a.u. for S_z , relative to the $N = 6$ and $S_z = 0$ a.u. values characterizing the ground electronic state of H_6 . This observation is consistent with the analytical results presented in the Supporting Information. As might have been anticipated, we find that the more controls are removed, the more severe the symmetry breaking becomes, as illustrated in Figure 1.

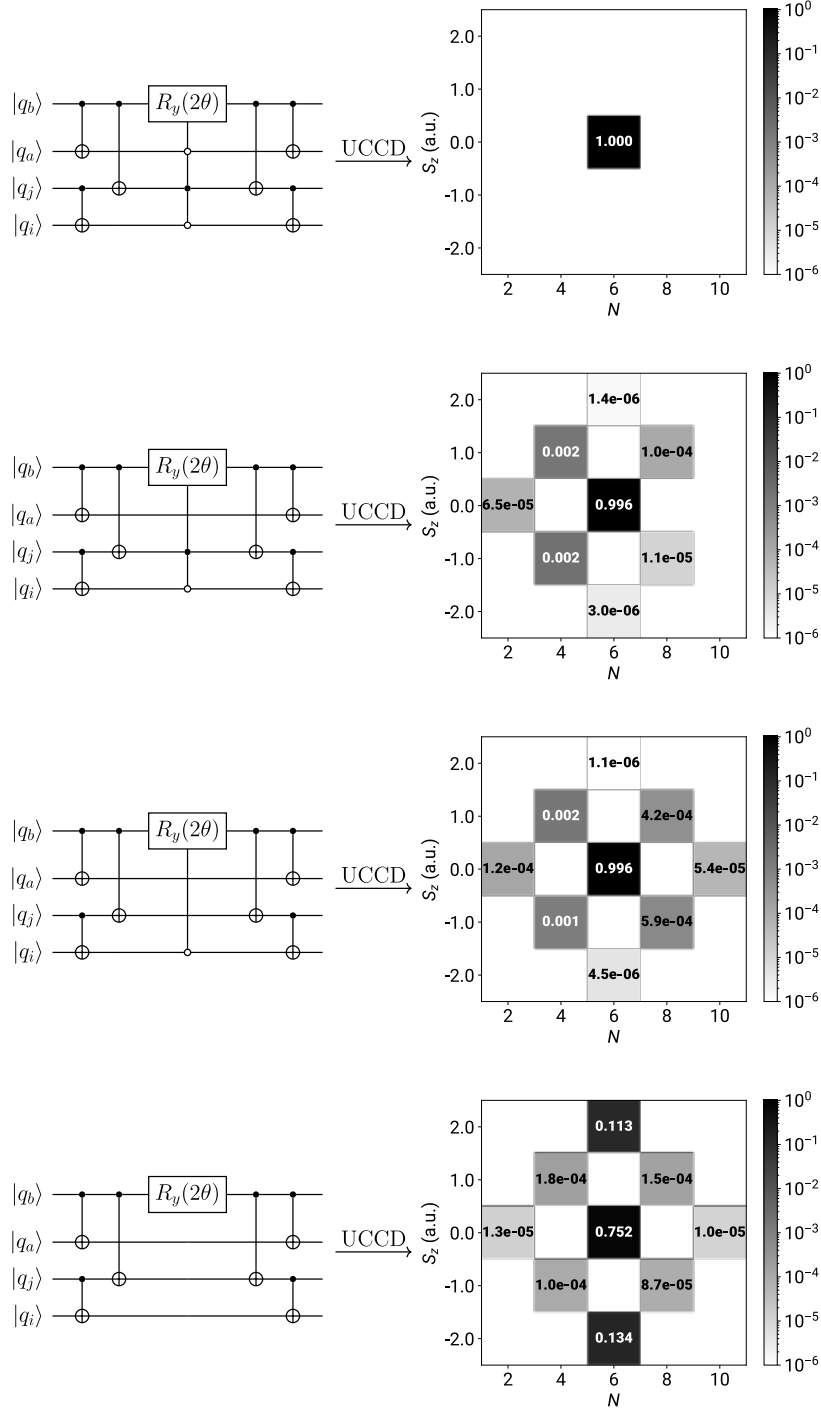


Figure 1: Illustration of the N - and S_z -symmetry breaking introduced by the removal of controls from the multiply controlled R_y gate appearing in the FEB/QEB quantum circuits. On the left we give the relevant qubit double excitation circuits and on the right we provide the contribution of each symmetry sector of the Fock space to the converged wavefunctions. Since spatial symmetry is conserved, only the totally symmetric part of the Fock space is considered. The depicted data resulted from VQE QEB-UCCD simulations of the H_6 /STO-6G linear chain with a separation between neighboring H atoms of 2.0 Å.

Consequently, the guiding principle in designing such approximate FEB/QEB quantum circuits has been to find a good compromise between reducing the CNOT count and minimizing the loss of accuracy in the computed energies and the breaking of symmetries in the final states. In the Supporting Information, we consider various approximate schemes, implemented in a local version of the QForte package.⁵⁰ We performed single-point selected PQE⁹ (SPQE) simulations for the challenging H₆/STO-6G linear chain with $R_{\text{H-H}} = 2.0 \text{ \AA}$. Recall that the SPQE algorithm typically relies on a complete pool of particle-hole excitation operators to iteratively construct the ansatz, eq (2), and the optimum parameters are obtained by enforcing the residual condition

$$r_\mu \equiv \langle \Phi_\mu | U^\dagger(\mathbf{t}) H U(\mathbf{t}) | \Phi \rangle = 0 \quad (5)$$

for all excited Slater determinants $|\Phi_\mu\rangle$ corresponding to the excitation operators κ_μ appearing in the ansatz unitary $U(\mathbf{t})$ (the details of the PQE and SPQE approaches can be found in refs 9 and 41). Based on these preliminary computations, the best balance is offered by the following recipe (see the Supporting Information for the details):

- Single and double excitations are treated fully [see panels (a) and (b) of Figure S6].
- For triple and quadruple excitations, only controls over qubits corresponding to occupied spinorbitals are retained in the multi-qubit-controlled R_y gate [see panels (c) and (d) of Figure S6].
- For pentuple and higher-rank excitations, all controls are removed [see Figure S6(e)], i.e., the multi-qubit-controlled R_y gate is replaced by its single-qubit analog.

In the case of higher-rank excitation operators, the above procedure reduces the scaling of the CNOT count with the excitation rank from exponential to linear. For qubit excitations, in particular, the number of CNOT gates becomes $4n - 2$, where n is the excitation rank.

To assess the effectiveness of the above approximation scheme, denoted as aFEB for

fermionic and aQEB for qubit excitations, and to compare it with the parent FEB/QEB quantum circuits across a wide range of correlation effects, we performed SPQE simulations of the symmetric dissociation of the $\text{H}_6/\text{STO-6G}$ linear chain. The grid of H–H distances used to sample the potential energy curve (PEC) was $R_{\text{H-H}} = 0.5, 0.6, \dots, 4.0 \text{ \AA}$. All SPQE simulations reported in this work utilized a full operator pool and micro- and macro-iteration thresholds of $10^{-5} E_h$ and $10^{-2} E_h$, respectively (see refs 9 and 41 for the details of the recently proposed SPQE algorithm). To ensure a lower number of residual element evaluations, the PQE micro-iterations employed the direct inversion of the iterative subspace^{51–53} (DIIS) accelerator and the maximum number of micro-iterations was set to 50. All correlated approaches were based on restricted Hartree–Fock references with the one- and two-electron integrals obtained from Psi4.⁵⁴

We begin the discussion of our numerical results by examining the ability of the aFEB-SPQE approach to reproduce the parent FEB-SPQE simulations and reduce the required computational resources. To that end, in Figure 2, we compare the energies, numbers of operators in the converged ansatz unitaries, CNOT counts, and numbers of residual element evaluations obtained with FEB-SPQE and aFEB-SPQE, characterizing the symmetric dissociation of the $\text{H}_6/\text{STO-6G}$ linear chain. A quick inspection of Figure 2 immediately reveals that aFEB-SPQE is both a highly accurate approximation to FEB-SPQE and computationally efficient. In the case of energetics, aFEB-SPQE faithfully reproduces the data of the full FEB-SPQE approach, being characterized by mean absolute, maximum absolute, and non-parallelity error values of 10, 32, and $53 \mu E_h$, respectively. As far as the computational resources are concerned, aFEB-SPQE captures practically the identical numbers of parameters when compared to FEB-SPQE [see panel (b) of Figure 2]. Nevertheless, as illustrated in Figure 2(c), aFEB-SPQE generates quantum circuits with significantly reduced numbers of CNOT gates than full FEB-SPQE. As might have been anticipated from the nature of the approximation, the disparity between the aFEB- and FEB-SPQE CNOT counts is dramatically increased as the strength of non-dynamic correlations increases, with aFEB-SPQE

requiring up to 4 times less CNOTs than its full FEB counterpart. Finally, the aFEB- and FEB-SPQE schemes require more or less the same numbers of residual element evaluations. Consequently, despite the drastic nature of the approximation in the quantum circuits, aFEB-SPQE accurately reproduces the FEB-SPQE energies and, by extension, those of full configuration interaction (FCI), but at a tiny fraction of the computational cost of its FEB-SPQE parent. This observation is true for the entire range of electron correlation effects characterizing the symmetric dissociation of the H_6 /STO-6G linear chain.

Despite the excellent performance in recovering the FEB-SPQE energetics, as already mentioned above and elaborated on in the Supporting Information, the approximations in the underlying quantum circuits defining the aFEB-SPQE approach result in the breaking of the particle number N and total spin projection S_z symmetries. It is, thus, worth examining the degree to which these symmetries are broken. As illustrated in Figure 3, the expectation values of the N and S_z operators are essentially identical to the eigenvalues of 6 and 0 a.u., respectively, characterizing the ground electronic state of the linear H_6 system. Indeed, the maximum unsigned errors are 2×10^{-5} in the case of N and 3×10^{-6} a.u. for S_z . However, due to the fact that the symmetry breaking introduces contaminants with both lower and higher eigenvalues of N and S_z , expectation values are not a good metric. By examining the error bars shown in Figure 3, given by the standard deviation $\sigma_A = \sqrt{\langle A^2 \rangle - \langle A \rangle^2}$, the following trend becomes apparent. In the weakly correlated regime, there is practically no symmetry breaking. As all H–H distances are symmetrically stretched, the standard deviations gradually increase in the recoupling region until they reach their maximum values, around $R_{H-H} = 2.5 \text{ \AA}$. Finally, as H_6 approaches its dissociation limit, the errors gradually decrease. This pattern directly correlates with the number of higher-than-double excitation operators in the ansatz, shown in Figure 2(b). This behavior is not surprising since the aFEB approximate scheme relies on a full implementation of singles and doubles, i.e., the higher-than-double excitation operators are the sole source of N - and S_z -symmetry contaminants. The maximum standard deviations of $\max(\sigma_N) = 0.011$ and $\max(\sigma_{S_z}) = 0.003$ a.u.

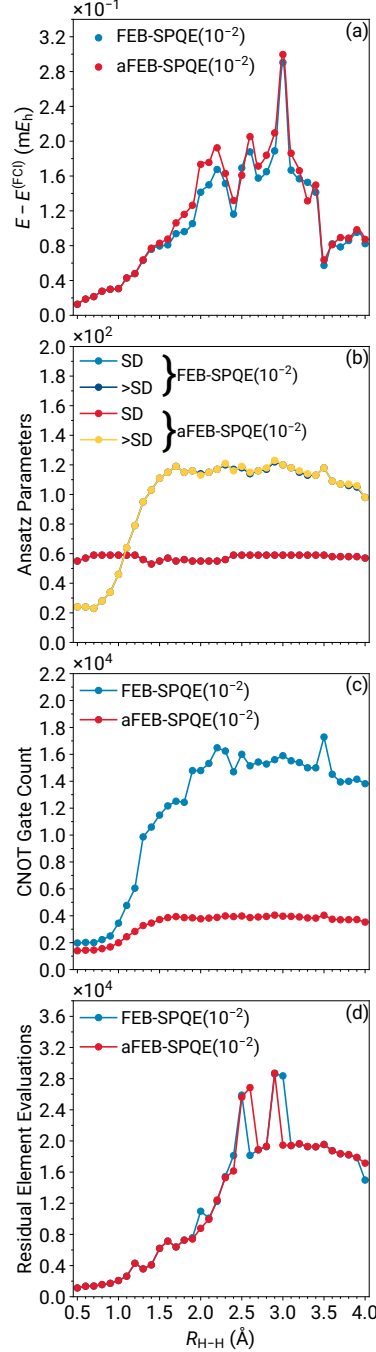


Figure 2: Errors relative to FCI [(a)], ansatz parameters [(b)], CNOT gate counts [(c)], and residual element evaluations [(d)] characterizing the FEB- and aFEB-SPQE simulations of the symmetric dissociation of the linear $H_6/STO-6G$ system. The “SD” and “>SD” symbols in the legend to panel (b) denote single or double (SD) or higher (>SD) excitation operators.

are, respectively, two and three orders of magnitude smaller than the distance of 1 between the neighboring eigenvalues of N and S_z . This observation provides further evidence sup-

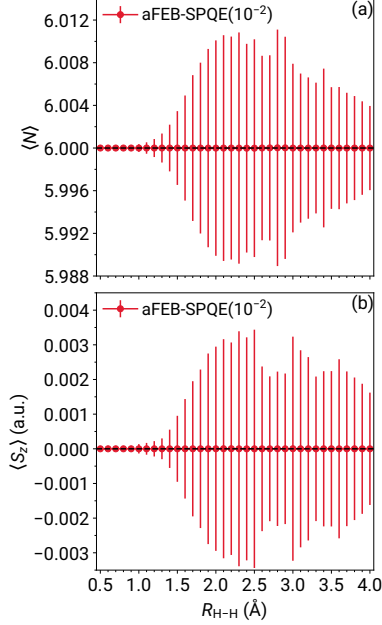


Figure 3: Expectation values of (a) the particle number N and (b) the projection of the total spin on the z axis S_z operators characterizing the aFEB-SPQE simulations of the symmetric dissociation of the linear $\text{H}_6/\text{STO-6G}$ system. The vertical lines denote standard deviations, computed as $\sigma_A = \sqrt{\langle A^2 \rangle - \langle A \rangle^2}$. The horizontal dashed lines denote the corresponding eigenvalues for the ground electronic state of the $\text{H}_6/\text{STO-6G}$ linear chain.

porting the notion that the aFEB scheme induces negligible symmetry breaking effects. As a definitive proof, we computed the weight of the totally symmetric Slater determinants with $N = 6$ and $S_z = 0$ in the final wavefunctions. Focusing on the $R_{\text{H-H}} = 2.5 \text{ \AA}$ and 2.8 \AA geometries, corresponding to $\max(\sigma_{S_z})$ and $\max(\sigma_N)$, respectively, we find that the weight of determinants having the correct symmetry properties are 99.998% and 99.999%.

Due to the use of a determinantal basis, the converged states resulting from FEB- and aFEB-SPQE simulations are not necessarily eigenfunctions of the square of the total spin operator, S^2 . Nevertheless, it is still interesting to examine how the $\langle S^2 \rangle$ and σ_{S^2} values are affected when one transitions from the parent FEB-SPQE scheme to its aFEB approximation. As depicted in Figure 4, aFEB-SPQE yields nearly identical $\langle S^2 \rangle$ and σ_{S^2} values with those obtained with the full FEB-SPQE approach. This further reinforces the fact that aFEB-SPQE is a high-fidelity approximation to FEB-SPQE.

Although here we focused on the aFEB-/FEB-SPQE pair, as shown in Figures S7–S9,

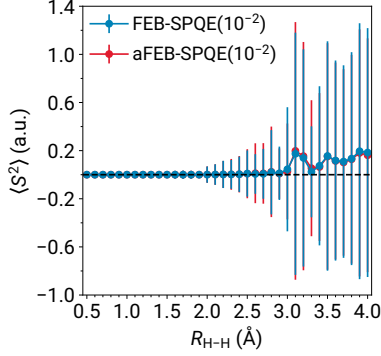


Figure 4: Expectation values of the total spin squared S^2 operator characterizing the FEB- and aFEB-SPQE simulations of the symmetric dissociation of the linear H_6 /STO-6G system. The vertical lines denote standard deviations, computed as $\sigma_A = \sqrt{\langle A^2 \rangle - \langle A \rangle^2}$. The horizontal dashed line denotes the corresponding eigenvalue for the ground electronic state of the H_6 /STO-6G linear chain.

similar observations can be made when examining the performance of the aQEB approximation to QEB-SPQE. In comparing the two approximate schemes among themselves (Figures S10 and S11), we notice that aQEB-SPQE typically produces quantum circuits with fewer CNOT gates than its fermionic counterpart, especially in situations characterized by stronger non-dynamic correlation effects. At the same time, however, aQEB-SPQE is typically less accurate than aFEB-SPQE and the symmetry breaking is more pronounced. These observations indicate that aFEB-SPQE achieves a favorable balance between minimizing the CNOT count and mitigating the loss of accuracy in energetics and symmetry breaking in the final states.

Our preliminary numerical results advocate that the aFEB scheme has several desirable properties of an approximation. It is highly accurate, reproducing the parent FEB-SPQE simulations with errors not exceeding a few microhartree. It has a low computational cost, reducing the number of CNOT gates compared to its already efficient FEB analog by 65%, on average. Furthermore, the aFEB quantum circuits are much simpler compared to their FEB counterparts, suggesting an easier hardware implementation. One aspect of aFEB-SPQE that we intend to examine in the future is its stability. Although preliminary single-point calculations for the H_6 ring, the H_8 linear chain, the linear BeH_2 system, and the

C_{2v} -symmetric insertion of Be to H_2 indicate that aFEB-SPQE behaves similarly to the case of the H_6 linear chain, a more thorough investigation is required. It is also worth exploring the usefulness of symmetry restoration^{55–57} within the various approximations considered in this work. As shown in our preliminary single-point calculations reported in Table S1, restoring the N and S_z symmetries in aFEB-/aQEB-SPQE has a negligible effect in the computed energies. This is due to the fact that the symmetry breaking in these approximations is practically insignificant. Nevertheless, symmetry restoration might prove useful in the context of more drastic approximations. In such cases, it might be possible to reduce the CNOT counts even further while still maintaining a high degree of accuracy in the computed energies.

Acknowledgement

This work is supported by the U.S. Department of Energy under Award No. DE-SC0019374.

Supporting Information Available

Details on the approximate fermionic- and qubit-excitation-based quantum circuits, analysis of the ensuing symmetry breaking, results of additional numerical simulations.

Numerical data generated in this study.

References

- (1) Reiher, M.; Wiebe, N.; Svore, K. M.; Wecker, D.; Troyer, M. Elucidating Reaction Mechanisms on Quantum Computers. *Proc. Natl. Acad. Sci. U.S.A.* **2017**, *114*, 7555–7560, DOI: 10.1073/pnas.1619152114.
- (2) Lee, S.; Lee, J.; Zhai, H.; Tong, Y.; Dalzell, A. M.; Kumar, A.; Helms, P.; Gray, J.; Cui, Z.-H.; Liu, W.; Kastoryano, M.; Babbush, R.; Preskill, J.; Reichman, D. R.; Camp-

- bell, E. T.; Valeev, E. F.; Lin, L.; Chan, G. K.-L. Is There Evidence for Exponential Quantum Advantage in Quantum Chemistry? 2022, arXiv:2208.02199. arXiv.org e-Print archive. <https://arxiv.org/abs/2208.02199>.
- (3) Peruzzo, A.; McClean, J.; Shadbolt, P.; Yung, M.-H.; Zhou, X.-Q.; Love, P. J.; Aspuru-Guzik, A.; O'Brien, J. L. A Variational Eigenvalue Solver on a Photonic Quantum Processor. *Nat. Commun.* **2014**, *5*, 4213, DOI: 10.1038/ncomms5213.
- (4) McClean, J. R.; Romero, J.; Babbush, R.; Aspuru-Guzik, A. The Theory of Variational Quantum-Classical Algorithms. *New J. Phys.* **2016**, *18*, 023023, DOI: 10.1088/1367-2630/18/2/023023.
- (5) Cerezo, M.; Arrasmith, A.; Babbush, R.; Benjamin, S. C.; Endo, S.; Fujii, K.; McClean, J. R.; Mitarai, K.; Yuan, X.; Cincio, L.; Coles, P. J. Variational Quantum Algorithms. *Nat. Rev. Phys.* **2021**, *3*, 625–644, DOI: 10.1038/s42254-021-00348-9.
- (6) Tilly, J.; Chen, H.; Cao, S.; Picozzi, D.; Setia, K.; Li, Y.; Grant, E.; Wossnig, L.; Rungger, I.; Booth, G. H.; Tennyson, J. The Variational Quantum Eigensolver: A Review of Methods and Best Practices. 2021, arXiv:2111.05176. arXiv.org e-Print archive. <https://arxiv.org/abs/2111.05176>.
- (7) Fedorov, D. A.; Peng, B.; Govind, N.; Alexeev, Y. VQE Method: A Short Survey and Recent Developments. *Mater. Theory* **2022**, *6*, 2, DOI: 10.1186/s41313-021-00032-6.
- (8) Smart, S. E.; Mazziotti, D. A. Quantum Solver of Contracted Eigenvalue Equations for Scalable Molecular Simulations on Quantum Computing Devices. *Phys. Rev. Lett.* **2021**, *126*, 070504, DOI: 10.1103/PhysRevLett.126.070504.
- (9) Stair, N. H.; Evangelista, F. A. Simulating Many-Body Systems with a Projective Quantum Eigensolver. *PRX Quantum* **2021**, *2*, 030301, DOI: 10.1103/PRXQuantum.2.030301.

- (10) Motta, M.; Sun, C.; Tan, A. T. K.; O'Rourke, M. J.; Ye, E.; Minnich, A. J.; ao, F. G. S. L. B.; Chan, G. K.-L. Determining Eigenstates and Thermal States on a Quantum Computer Using Quantum Imaginary Time Evolution. *Nat. Phys.* **2020**, *16*, 205–210, DOI: 10.1038/s41567-019-0704-4.
- (11) Sun, S.-N.; Motta, M.; Tazhigulov, R. N.; Tan, A. T. K.; Chan, G. K.-L.; Minnich, A. J. Quantum Computation of Finite-Temperature Static and Dynamical Properties of Spin Systems Using Quantum Imaginary Time Evolution. *PRX Quantum* **2021**, *2*, 010317, DOI: 10.1103/PRXQuantum.2.010317.
- (12) McClean, J. R.; Kimchi-Schwartz, M. E.; Carter, J.; de Jong, W. A. Hybrid Quantum-Classical Hierarchy for Mitigation of Decoherence and Determination of Excited States. *Phys. Rev. A* **2017**, *95*, 042308, DOI: 10.1103/PhysRevA.95.042308.
- (13) Parrish, R. M.; McMahon, P. L. Quantum Filter Diagonalization: Quantum Eigendecomposition without Full Quantum Phase Estimation. 2019, arXiv:1909.08925v1. arXiv.org e-Print archive. <https://arxiv.org/abs/1909.08925v1>.
- (14) Stair, N. H.; Huang, R.; Evangelista, F. A. A Multireference Quantum Krylov Algorithm for Strongly Correlated Electrons. *J. Chem. Theory Comput.* **2020**, *16*, 2236–2245, DOI: 10.1021/acs.jctc.9b01125.
- (15) Huggins, W. J.; Lee, J.; Baek, U.; O'Gorman, B.; Whaley, K. B. A Non-Orthogonal Variational Quantum Eigensolver. *New J. Phys.* **2020**, *22*, 073009, DOI: 10.1088/1367-2630/ab867b.
- (16) Kutzelnigg, W. In *Methods of Electronic Structure Theory*; Schaefer, H. F., III, Ed.; Springer: Boston, 1977; pp 129–188, DOI: 10.1007/978-1-4757-0887-5_5.
- (17) Kutzelnigg, W. Quantum Chemistry in Fock Space. I. The Universal Wave and Energy Operators. *J. Chem. Phys.* **1982**, *77*, 3081–3097, DOI: 10.1063/1.444231.

- (18) Kutzelnigg, W.; Koch, S. Quantum Chemistry in Fock Space. II. Effective Hamiltonians in Fock Space. *J. Chem. Phys.* **1983**, *79*, 4315–4335, DOI: 10.1063/1.446313.
- (19) Kutzelnigg, W. Quantum Chemistry in Fock Space. III. Particle-Hole Formalism. *J. Chem. Phys.* **1984**, *80*, 822–830, DOI: 10.1063/1.446736.
- (20) Bartlett, R. J.; Kucharski, S. A.; Noga, J. Alternative Coupled-Cluster Ansätze II. The Unitary Coupled-Cluster Method. *Chem. Phys. Lett.* **1989**, *155*, 133–140, DOI: 10.1016/S0009-2614(89)87372-5.
- (21) Szalay, P. G.; Nooijen, M.; Bartlett, R. J. Alternative Ansätze in Single Reference Coupled-Cluster Theory. III. A Critical Analysis of Different Methods. *J. Chem. Phys.* **1995**, *103*, 281–298, DOI: 10.1063/1.469641.
- (22) Taube, A. G.; Bartlett, R. J. New Perspectives on Unitary Coupled-Cluster Theory. *Int. J. Quantum Chem.* **2006**, *106*, 3393–3401, DOI: 10.1002/qua.21198.
- (23) Cooper, B.; Knowles, P. J. Benchmark Studies of Variational, Unitary and Extended Coupled Cluster Methods. *J. Chem. Phys.* **2010**, *133*, 234102, DOI: 10.1063/1.3520564.
- (24) Evangelista, F. A. Alternative Single-Reference Coupled Cluster Approaches for Multireference Problems: The Simpler, the Better. *J. Chem. Phys.* **2011**, *134*, 224102, DOI: 10.1063/1.3598471.
- (25) Harsha, G.; Shiozaki, T.; Scuseria, G. E. On the Difference Between Variational and Unitary Coupled Cluster Theories. *J. Chem. Phys.* **2018**, *148*, 044107, DOI: 10.1063/1.5011033.
- (26) Filip, M.-A.; Thom, A. J. W. A Stochastic Approach to Unitary Coupled Cluster. *J. Chem. Phys.* **2020**, *153*, 214106, DOI: 10.1063/5.0026141.

- (27) Freericks, J. K. Operator Relationship between Conventional Coupled Cluster and Unitary Coupled Cluster. *Symmetry* **2022**, *14*, 494, DOI: 10.3390/sym14030494.
- (28) Anand, A.; Schleich, P.; Alperin-Lea, S.; Jensen, P. W. K.; Sim, S.; Diaz-Tinoco, M.; Kottmann, J. S.; Degroote, M.; Izmaylov, A. F.; Aspuru-Guzik, A. A Quantum Computing View on Unitary Coupled Cluster Theory. *Chem. Soc. Rev.* **2022**, *51*, 1659–1684, DOI: 10.1039/d1cs00932j.
- (29) Coester, F. Bound States of a Many-Particle System. *Nucl. Phys.* **1958**, *7*, 421–424, DOI: 10.1016/0029-5582(58)90280-3.
- (30) Coester, F.; Kümmel, H. Short-Range Correlations in Nuclear Wave Functions. *Nucl. Phys.* **1960**, *17*, 477–485, DOI: 10.1016/0029-5582(60)90140-1.
- (31) Čížek, J. On the Correlation Problem in Atomic and Molecular Systems. Calculation of Wavefunction Components in Ursell-Type Expansion Using Quantum-Field Theoretical Methods. *J. Chem. Phys.* **1966**, *45*, 4256–4266, DOI: 10.1063/1.1727484.
- (32) Čížek, J. On the Use of the Cluster Expansion and the Technique of Diagrams in Calculations of Correlation Effects in Atoms and Molecules. *Adv. Chem. Phys.* **1969**, *14*, 35–89, DOI: 10.1002/9780470143599.ch2.
- (33) Čížek, J.; Paldus, J. Correlation Problems in Atomic and Molecular Systems III. Rederivation of the Coupled-Pair Many-Electron Theory Using the Traditional Quantum Chemical Methods. *Int. J. Quantum Chem.* **1971**, *5*, 359–379, DOI: 10.1002/qua.560050402.
- (34) Paldus, J.; Čížek, J.; Shavitt, I. Correlation Problems in Atomic and Molecular Systems. IV. Extended Coupled-Pair Many-Electron Theory and Its Application to the BH_3 Molecule. *Phys. Rev. A* **1972**, *5*, 50–67, DOI: 10.1103/PhysRevA.5.50.

- (35) Evangelista, F. A.; Chan, G. K.-L.; Scuseria, G. E. Exact Parameterization of Fermionic Wave Functions via Unitary Coupled Cluster Theory. *J. Chem. Phys.* **2019**, *151*, 244112, DOI: 10.1063/1.5133059.
- (36) Yordanov, Y. S.; Arvidsson-Shukur, D. R. M.; Barnes, C. H. W. Efficient Quantum Circuits for Quantum Computational Chemistry. *Phys. Rev. A* **2020**, *102*, 062612, DOI: 10.1103/PhysRevA.102.062612.
- (37) Yordanov, Y. S.; Armaos, V.; Barnes, C. H. W.; Arvidsson-Shukur, D. R. M. Qubit-Excitation-Based Adaptive Variational Quantum Eigensolver. *Commun. Phys.* **2021**, *4*, 228, DOI: 10.1038/s42005-021-00730-0.
- (38) Xia, R.; Kais, S. Qubit Coupled Cluster Singles and Doubles Variational Quantum Eigensolver Ansatz for Electronic Structure Calculations. *Quantum Sci. Technol.* **2021**, *6*, 015001, DOI: 10.1088/2058-9565/abbc74.
- (39) Mazziotti, D. A.; Smart, S. E.; Mazziotti, A. R. Quantum Simulation of Molecules without Fermionic Encoding of the Wave Function. *New J. Phys.* **2021**, *23*, 113037, DOI: 10.1088/1367-2630/ac3573.
- (40) Smart, S. E.; Mazziotti, D. A. Many-Fermion Simulation from the Contracted Quantum Eigensolver without Fermionic Encoding of the Wave Function. *Phys. Rev. A* **2022**, *105*, 062424, DOI: 10.1103/PhysRevA.105.062424.
- (41) Magoulas, I.; Evangelista, F. A. CNOT-Efficient Quantum Circuits for Arbitrary Rank Many-Body Fermionic and Qubit Excitations. *J. Chem. Theory Comput.* **2023**, *19*, 822–836, DOI: 10.1021/acs.jctc.2c01016.
- (42) Xu, L.; Freericks, J. K. Efficient Application of the Factorized Form of the Unitary Coupled-Cluster Ansatz for the Variational Quantum Eigensolver Algorithm by Using Linear Combination of Unitaries. 2023, arXiv:2302.08679. arXiv.org e-Print archive. <https://arxiv.org/abs/2302.08679>.

- (43) Quantum Computer Datasheet. Google, 2021.
- (44) Nooijen, M. Can the Eigenstates of a Many-Body Hamiltonian Be Represented Exactly Using a General Two-Body Cluster Expansion? *Phys. Rev. Lett.* **2000**, *84*, 2108–2111, DOI: 10.1103/PhysRevLett.84.2108.
- (45) Nakatsuji, H. Structure of the Exact Wave Function. *J. Chem. Phys.* **2000**, *113*, 2949–2956, DOI: 10.1063/1.1287275.
- (46) Maslov, D. Advances of using Relative-Phase Toffoli Gates with an Application to Multiple Control Toffoli Optimization. *Phys. Rev. A* **2016**, *93*, 022311, DOI: 10.1103/PhysRevA.93.022311.
- (47) da Silva, A. J.; Park, D. K. Linear-Depth Quantum Circuits for Multiqubit Controlled Gates. *Phys. Rev. A* **2022**, *106*, 042602, DOI: 10.1103/PhysRevA.106.042602.
- (48) Vale, R.; Azevedo, T. M. D.; Araújo, I. C. S.; Araujo, I. F.; da Silva, A. J. Decomposition of Multi-Controlled Special Unitary Single-Qubit Gates. 2023, arXiv:2302.06377. arXiv.org e-Print archive. <https://arxiv.org/abs/2302.06377>.
- (49) Hehre, W. J.; Stewart, R. F.; Pople, J. A. Self-Consistent Molecular-Orbital Methods. I. Use of Gaussian Expansions of Slater-Type Atomic Orbitals. *J. Chem. Phys.* **1969**, *51*, 2657–2664, DOI: 10.1063/1.1672392.
- (50) Stair, N. H.; Evangelista, F. A. QFort: An Efficient State-Vector Emulator and Quantum Algorithms Library for Molecular Electronic Structure. *J. Chem. Theory Comput.* **2022**, *18*, 1555–1568, DOI: 10.1021/acs.jctc.1c01155.
- (51) Pulay, P. Convergence Acceleration of Iterative Sequences. The Case of SCF Iteration. *Chem. Phys. Lett.* **1980**, *73*, 393–398, DOI: 10.1016/0009-2614(80)80396-4.
- (52) Pulay, P. Improved SCF Convergence Acceleration. *J. Comput. Chem.* **1982**, *3*, 556–560, DOI: 10.1002/jcc.540030413.

- (53) Scuseria, G. E.; Lee, T. J.; Schaefer III, H. F. Accelerating the Convergence of the Coupled-Cluster Approach. *Chem. Phys. Lett.* **1986**, *130*, 236–239, DOI: 10.1016/0009-2614(86)80461-4.
- (54) Smith, D. G. A.; Burns, L. A.; Simmonett, A. C.; Parrish, R. M.; Schieber, M. C.; Galvelis, R.; Kraus, P.; Kruse, H.; Remigio, R. D.; Alenaizan, A.; James, A. M.; Lehtola, S.; Misiewicz, J. P.; Scheurer, M.; Shaw, R. A.; Schriber, J. B.; Xie, Y.; Glick, Z. L.; Sirianni, D. A.; O’Brien, J. S.; Waldrop, J. M.; Kumar, A.; Hohenstein, E. G.; Pritchard, B. P.; Brooks, B. R.; Schaefer III, H. F.; Sokolov, A. Y.; Patkowski, K.; DePrince III, A. E.; Bozkaya, U.; King, R. A.; Evangelista, F. A.; Turney, J. M.; Crawford, T. D.; Sherrill, C. D. PSI4 1.4: Open-Source Software for High-Throughput Quantum Chemistry. *J. Chem. Phys.* **2020**, *152*, 184108, DOI: 10.1063/5.0006002.
- (55) Tsuchimochi, T.; Mori, Y.; Ten-no, S. L. Spin Projection for Quantum Computation: A Low-Depth Approach to Strong Correlation. *Phys. Rev. Res.* **2020**, *2*, 043142, DOI: 10.1103/PhysRevResearch.2.043142.
- (56) Khamoshi, A.; Evangelista, F. A.; Scuseria, G. E. Correlating AGP on a Quantum Computer. *Quantum Sci. Technol.* **2021**, *6*, 014004, DOI: 10.1088/2058-9565/abc1bb.
- (57) Khamoshi, A.; Chen, G. P.; Evangelista, F. A.; Scuseria, G. E. AGP-Based Unitary Coupled Cluster Theory for Quantum Computers. *Quantum Sci. Technol.* **2023**, *8*, 015006, DOI: 10.1088/2058-9565/ac93ae.

Supporting Information:
Linear-Scaling Quantum Circuits for
Computational Chemistry

Ilias Magoulas* and Francesco A. Evangelista*

*Department of Chemistry and Cherry Emerson Center for Scientific Computation,
Emory University, Atlanta, Georgia 30322, USA*

E-mail: ilias.magoulas@emory.edu; francesco.evangelista@emory.edu

This Supporting Information document is organized as follows. In Section S1 we describe the various approximate fermionic- (FEB) and qubit-excitation-based (QEB) quantum circuits considered in this study, including an analysis of the ensuing symmetry breaking. Section S2 provides, in a graphical form, the results of our additional numerical simulations. In particular, in Section S2.1 we assess the effectiveness of the aQEB approximation to QEB-SPQE(10^{-2}) for the symmetric dissociation of the H_6 /STO-6G linear chain. Finally, in Section S2.2, we compare the performance of the aFEB- and aQEB-SPQE(10^{-2}) approximations for the symmetric dissociation of the H_6 /STO-6G linear chain.

The numerical data generated in this study can be found in the Excel file that forms part of the present Supporting Information.

S1 Approximate FEB/QEB Quantum Circuits

In this section, we discuss the various approximate FEB/QEB quantum circuits explored in this study. Figure S1 depicts the full QEB [panel (a)] and FEB [panel (b)] quantum circuits performing n -tuple qubit and fermionic excitations, respectively. As shown in ref 41 of the main text, the decomposition of the multi-qubit-controlled R_y gate introduces an exponential number of CNOT gates, rendering it the main source of CNOTs. This is still true even if one adopts the more efficient implementations of the multiply controlled R_y gate introduced in refs 46–48. The number of CNOTs can be dramatically reduced by adopting approximate forms of the multi-qubit-controlled R_y gate in which certain controls are removed.

Without loss of generality, to illustrate the consequences of approximate implementations of the multi-qubit-controlled R_y gate, we focus on the simpler case of QEB doubles. The full

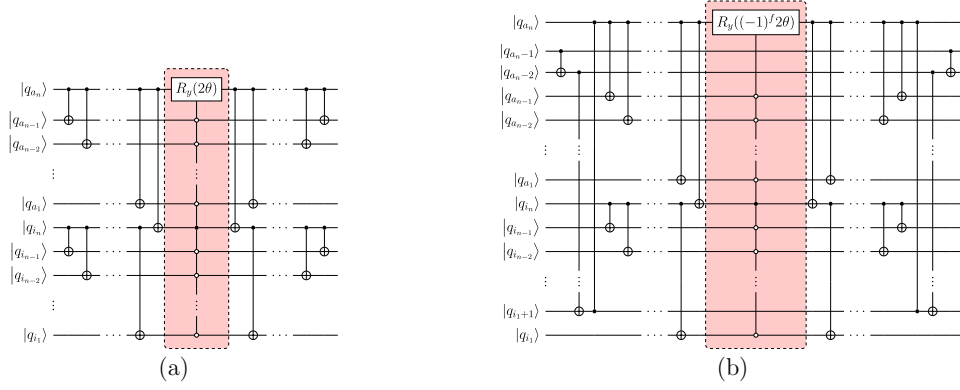


Figure S1: CNOT-efficient quantum circuits performing (a) qubit and (b) fermionic n -tuple particle-hole excitations. Indices i_1, \dots, i_n (a_1, \dots, a_n) correspond to spinorbitals occupied (unoccupied) in the reference Slater determinant. The parameter f controlling the sign of the rotation angle depends on the excitation rank n as follows: $f = 0$ for $n = 1, 4, 5, 8, 9, \dots$ and $f = 1$ for $n = 2, 3, 6, 7, \dots$. In both circuits, the multi-qubit-controlled R_y gate, shaded in red color, is the main source of CNOT gates. The open circles denote anticontrol qubits

circuit, shown in Figure S2, implements a double qubit excitation exactly, i.e.,

$$e^{Q_{ij}^{ab}} |q_i q_j q_a q_b\rangle = \begin{cases} \cos(\theta) |1_i 1_j 0_a 0_b\rangle + \sin(\theta) |0_i 0_j 1_a 1_b\rangle, & q_i = q_j = 1, q_a = q_b = 0 \\ -\sin(\theta) |1_i 1_j 0_a 0_b\rangle + \cos(\theta) |0_i 0_j 1_a 1_b\rangle, & q_i = q_j = 0, q_a = q_b = 1 \\ |q_i q_j q_a q_b\rangle, & \text{otherwise} \end{cases} \quad (1)$$

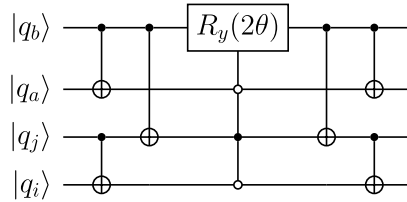


Figure S2: QEB quantum circuit performing a qubit double particle-hole excitation, $\exp(Q_{ij}^{ab})$.

Essentially, the QEB doubles circuit performs a continuous exchange of the $|1_i 1_j 0_a 0_b\rangle$

and $|0_i 0_j 1_a 1_b\rangle$ states. Figure S3 depicts the crudest approximation in which all controls have been removed, replacing the multi-qubit-controlled R_y gate by its single-qubit counterpart.

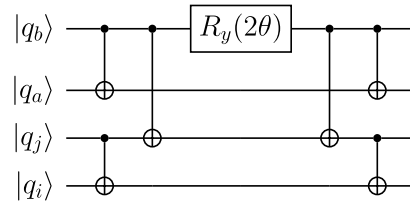


Figure S3: In the crudest approximation to the QEB quantum circuit shown in Figure S2, the multi-qubit-controlled R_y gate is replaced by its single-qubit counterpart.

It is straightforward to show that this quantum circuit performs the operation

$$U |q_i q_j q_a q_b\rangle = \left\{ \begin{array}{ll} \cos(\theta) |0_i 0_j 0_a 0_b\rangle + \sin(\theta) |1_i 1_j 1_a 1_b\rangle, & q_i = q_j = q_a = q_b = 0 \\ -\sin(\theta) |0_i 0_j 0_a 0_b\rangle + \cos(\theta) |1_i 1_j 1_a 1_b\rangle, & q_i = q_j = q_a = q_b = 1 \\ \cos(\theta) |1_i 0_j 0_a 0_b\rangle + \sin(\theta) |0_i 1_j 1_a 1_b\rangle, & q_i = 1, q_j = q_a = q_b = 0 \\ -\sin(\theta) |1_i 0_j 0_a 0_b\rangle + \cos(\theta) |0_i 1_j 1_a 1_b\rangle, & q_i = 0, q_j = q_a = q_b = 1 \\ \cos(\theta) |0_i 1_j 0_a 0_b\rangle + \sin(\theta) |1_i 0_j 1_a 1_b\rangle, & q_j = 1, q_i = q_a = q_b = 0 \\ -\sin(\theta) |0_i 1_j 0_a 0_b\rangle + \cos(\theta) |1_i 0_j 1_a 1_b\rangle, & q_j = 0, q_i = q_a = q_b = 1 \\ \cos(\theta) |1_i 1_j 0_a 0_b\rangle + \sin(\theta) |0_i 0_j 1_a 1_b\rangle, & q_i = q_j = 1, q_a = q_b = 0 \\ -\sin(\theta) |1_i 1_j 0_a 0_b\rangle + \cos(\theta) |0_i 0_j 1_a 1_b\rangle, & q_i = q_j = 0, q_a = q_b = 1 \\ \cos(\theta) |0_i 0_j 1_a 0_b\rangle + \sin(\theta) |1_i 1_j 0_a 1_b\rangle, & q_a = 1, q_i = q_j = q_b = 0 \\ -\sin(\theta) |0_i 0_j 1_a 0_b\rangle + \cos(\theta) |1_i 1_j 0_a 1_b\rangle, & q_a = 0, q_i = q_j = q_b = 1 \\ \cos(\theta) |1_i 0_j 1_a 0_b\rangle + \sin(\theta) |0_i 1_j 0_a 1_b\rangle, & q_i = q_a = 1, q_j = q_b = 0 \\ -\sin(\theta) |1_i 0_j 1_a 0_b\rangle + \cos(\theta) |0_i 1_j 0_a 1_b\rangle, & q_i = q_a = 0, q_j = q_b = 1 \\ \cos(\theta) |0_i 1_j 1_a 0_b\rangle + \sin(\theta) |1_i 0_j 0_a 1_b\rangle, & q_i = q_b = 0, q_j = q_a = 1 \\ -\sin(\theta) |0_i 1_j 1_a 0_b\rangle + \cos(\theta) |1_i 0_j 0_a 1_b\rangle, & q_i = q_b = 1, q_j = q_a = 0 \\ \cos(\theta) |1_i 1_j 1_a 0_b\rangle + \sin(\theta) |0_i 0_j 0_a 1_b\rangle, & q_i = q_j = q_a = 1, q_b = 0 \\ -\sin(\theta) |1_i 1_j 1_a 0_b\rangle + \cos(\theta) |0_i 0_j 0_a 1_b\rangle, & q_i = q_j = q_a = 0, q_b = 1 \end{array} \right. \quad (2)$$

The unitary operator U that performs the above continuous exchanges is

$$U = \underbrace{e^{\theta Q^{ijab}}}_{N\pm 4} \underbrace{e^{\theta Q_i^{ab}} e^{\theta Q_j^{ab}} e^{\theta Q_a^{ijb}} e^{\theta Q_b^{ija}}}_{N\pm 2} \underbrace{e^{\theta Q_{ia}^{jb}} e^{\theta Q_{ja}^{ib}} e^{\theta Q_{ij}^{ab}}}_{N}. \quad (3)$$

May break S_z symmetry: $M_S, M_S \pm 1, M_S \pm 2$

Examination of eq (3) reveals that U is the product of eight exponentials. Of these, five

violate the particle number (N) symmetry, attaching/ionizing either 2 or 4 electrons. At the same time, the first seven exponentials in eq (3) have the potential to break the total spin projected on the z axis (S_z) symmetry, introducing contaminants with $M_S \pm 1$ and $M_S \pm 2$. Which of the seven exponentials introduce S_z -symmetry contaminants depends on the m_s values of the spinorbitals involved in a given excitation process. Note, however, that spatial symmetry is retained.

In searching for an approximation scheme, it is crucial to not only minimize the CNOT count, but also keep the loss of accuracy in the computed energies and breaking of symmetry in the final states to a minimum. In Table S1, we considered 8 such approaches and applied them to the H_6 /STO-6G linear chain, a prototypical strongly correlated system. In this preliminary numerical exploration, we focused on the geometry in which the separation between neighboring H atoms is $R_{H-H} = 2.0 \text{ \AA}$, the largest distance considered in our earlier study.⁴¹ A simple inspection of Table S1 reveals that approximation schemes with a full treatment of singles and doubles reproduce the results of the parent FEB- and QEB-SPQE methods within a fraction of a millihartree. At the same time, the symmetry breaking introduced by these approaches is practically negligible, as evidenced by the standard deviations of N and S_z , as well as the contributions of the various symmetry sectors of the Fock space in the converged wavefunctions, shown in Figures S4 and S5. The necessity of treating single and double excitations fully, in particular the latter, is not a coincidence. Based on single-point FEB-SPQE calculations of other systems characterized by significant non-dynamic correlations, including the H_6 ring, the H_8 linear chain, the linear BeH_2 system, and the C_{2v} -symmetric insertion of Be to H_2 , the largest double-excitation amplitudes were about 10 times greater than their higher-rank counterparts. Out of the five approximation schemes that worked well, the one that we selected to test further in the main text is defined in Figure S6. Based on the preliminary data collected in Table S1, this scheme, abbreviated as aFEB and aQEB for fermionic and qubit excitations, respectively, offers the best balance between minimizing the CNOT count and mitigating the loss of accuracy in energetics and

symmetry breaking in the final states.

Table S1: Total electronic energies (in E_h), expectation values $\langle A \rangle$ and standard deviations σ_A of the particle number N , z -component of total spin S_z , and total spin squared S^2 operators (in a.u.), CNOT counts, and numbers of parameters characterizing the various full and approximate SQPE(10^{-2}) computations of H_6 /STO-6G with $R_{H-H} = 2.0 \text{ \AA}$.

Scheme	E	E_{pure}^a	$\langle N \rangle$	σ_N	$\langle S_z \rangle$	σ_{S_z}	$\langle S^2 \rangle$	σ_{S^2}	CNOTs	Parameters
FEB										
full ^b	-2.873932	-2.873932	6.000000	0.000000	0.000000	0.000000	0.000788	0.067510	14794	169
SD-full+occ ^c	-2.873908	-2.873931	5.999994	0.010081	0.000001	0.002952	0.000830	0.068874	4034	169
SD-full+TQ-occ ^d	-2.873900	-2.873922	5.999994	0.010099	0.000001	0.002946	0.000816	0.067949	3774	168
SD-full+unocc ^e	-2.873885	-2.873921	5.999994	0.013759	0.000001	0.002696	0.000794	0.067088	3296	168
SD-full+TQ-unocc ^f	-2.873884	-2.873921	5.999994	0.013721	0.000001	0.002690	0.000794	0.067093	3184	168
SD-full ^g	-2.873695	-2.873917	6.000013	0.027742	-0.000051	0.016882	0.001277	0.081575	2582	168
occ ^h	-2.861721	-2.867900	5.995097	0.139851	-0.001202	0.068937	0.383478	1.457258	3778	167
unocc ⁱ	-2.857341	-2.862585	6.002553	0.132236	-0.001621	0.060996	0.539628	1.706678	2810	162
min ^j	-2.787782	-2.836626	6.005907	0.249094	0.116015	0.882393	1.283279	2.437863	2094	161
QEB										
full ^b	-2.873933	-2.873933	6.000000	0.000000	0.000000	0.000000	0.002119	0.076628	14988	178
SD-full+occ ^c	-2.873904	-2.873949	6.000035	0.015015	0.000009	0.004386	0.001892	0.068447	3726	179
SD-full+TQ-occ ^d	-2.873895	-2.873944	6.000036	0.015420	0.000008	0.004631	0.001747	0.071800	3502	179
SD-full+unocc ^e	-2.873863	-2.873929	5.999952	0.016943	-0.000002	0.005175	0.001884	0.071776	2948	178
SD-full+TQ-unocc ^f	-2.873859	-2.873927	5.999953	0.017116	-0.000001	0.005307	0.001889	0.072632	2836	178
SD-full ^g	-2.873390	-2.873824	5.999976	0.037654	-0.000049	0.021261	0.002157	0.091124	2180	178
occ ^h	-2.864504	-2.868381	5.996943	0.112104	-0.000072	0.054616	0.336046	1.370817	3388	170
unocc ⁱ	-2.860408	-2.861957	6.000399	0.076798	0.000054	0.034511	0.684714	1.903075	2202	152
min ^j	-2.784765	-2.830128	5.996454	0.193159	0.113565	0.916424	1.468346	2.564975	1578	161

^a These energies were obtained as the expectation value of the Hamiltonian with respect to the state in which the N - and S_z -symmetry contaminants are removed and the resulting wavefunction is normalized. ^b Full FEB/QEB circuits; no approximations. ^c Full FEB/QEB circuits for singles and doubles; for higher-than-double excitations only controls over occupied spinorbitals are retained. ^d Full FEB/QEB circuits for singles and doubles, for triples and quadruples only controls over occupied spinorbitals are retained; for pentuples and higher-rank excitations all controls are removed. ^e Full FEB/QEB circuits for singles and doubles; for higher-than-double excitations only controls over unoccupied spinorbitals are retained. ^f Full FEB/QEB circuits for singles and doubles, for triples and quadruples only controls over unoccupied spinorbitals are retained; for pentuples and higher-rank excitations all controls are removed. ^g Full FEB/QEB circuits for singles and doubles; for higher-than-double excitations all controls are removed. ^h Only controls over occupied spinorbitals are retained. ⁱ Only controls over unoccupied spinorbitals are retained. ^j All controls are removed.

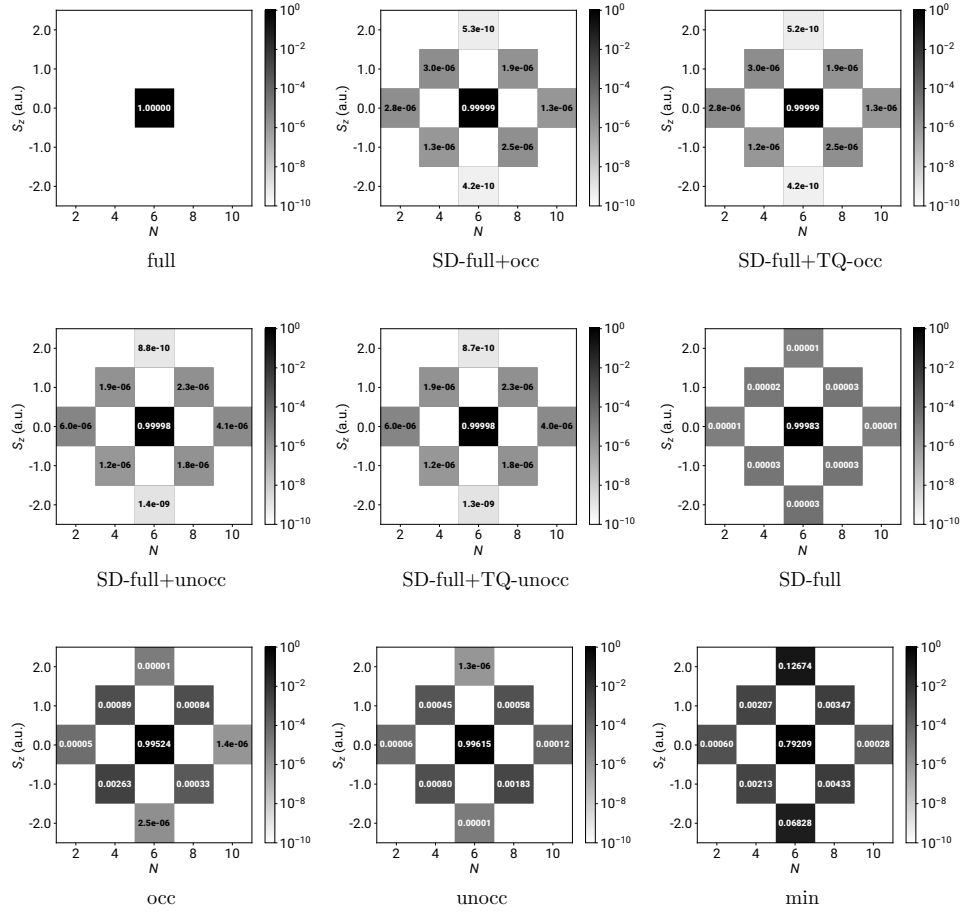


Figure S4: Contributions of the various symmetry sectors of the Fock space to the converged wavefunctions characterizing the various full and approximate FEB-SQPE(10^{-2}) computations of H_6 /STO-6G with $R_{H-H} = 2.0 \text{ \AA}$. The definitions of the various schemes can be found in the footnotes to Table S1. Note that all depicted symmetry sectors are totally symmetric since spatial symmetry is preserved.

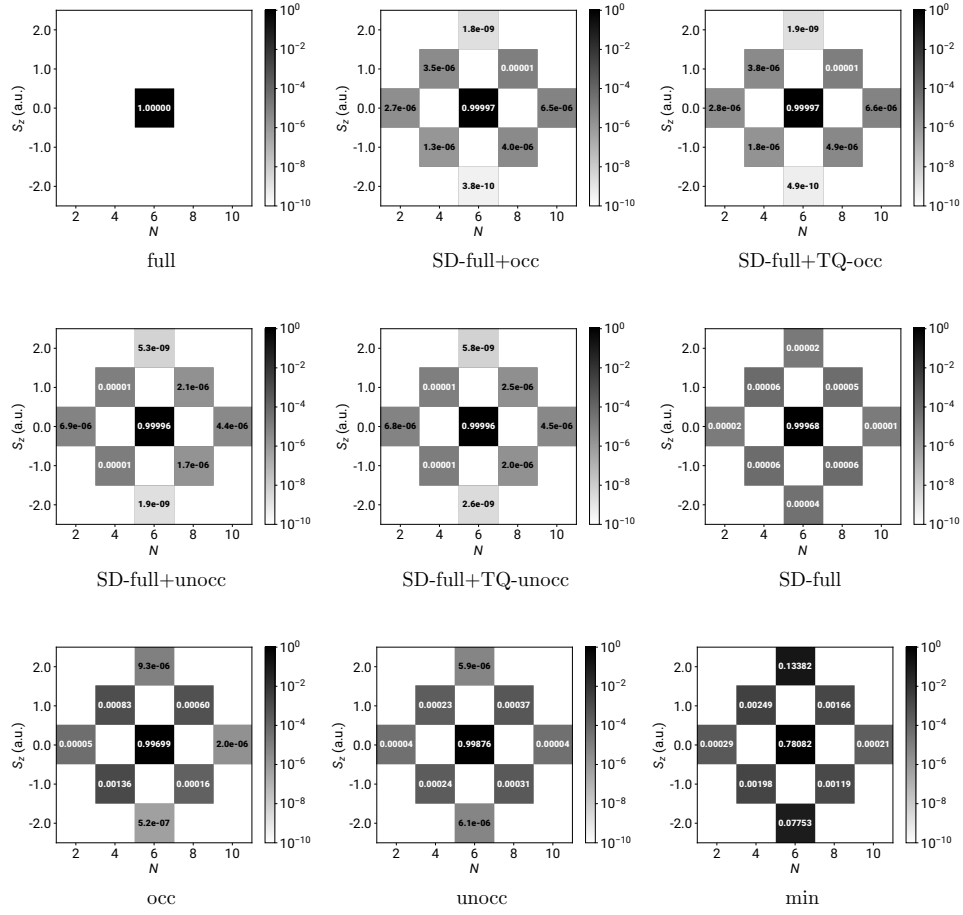


Figure S5: Contributions of the various symmetry sectors of the Fock space to the converged wavefunctions characterizing the various full and approximate QEB-SQPE(10^{-2}) computations of H_6 /STO-6G with $R_{H-H} = 2.0 \text{ \AA}$. The definitions of the various schemes can be found in the footnotes to Table S1. Note that all depicted symmetry sectors are totally symmetric since spatial symmetry is preserved.

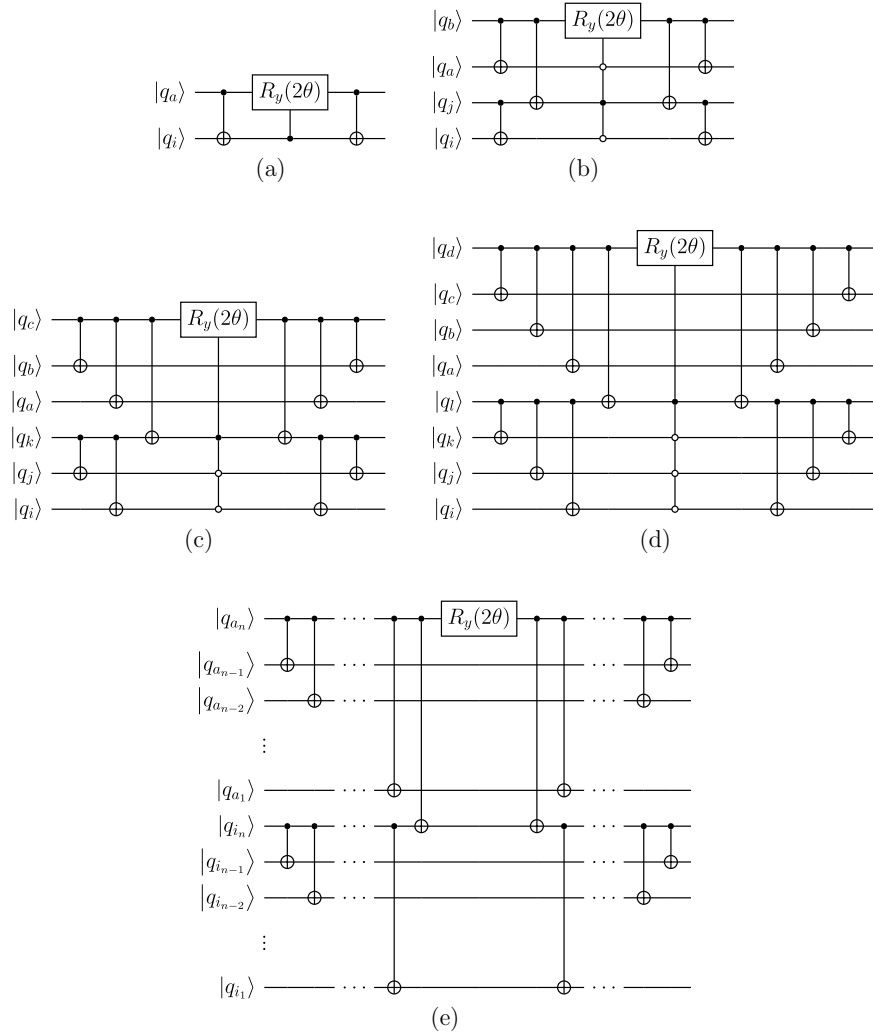


Figure S6: Quantum circuits defining the aQEB scheme. Single (a) and double (b) excitations are treated fully. For triple (c) and quadruple (d) excitations, only controls over qubits corresponding to occupied orbitals are retained in the multi-qubit-controlled R_y gate. For pentuple and higher-rank excitations (e), all controls are removed, i.e., the multi-qubit-controlled R_y gate is replaced by its single-qubit counterpart. The aFEB scheme is defined in a similar manner.

S2 Results of Additional Numerical Simulations

S2.1 QEB-SPQE vs aQEB-SPQE

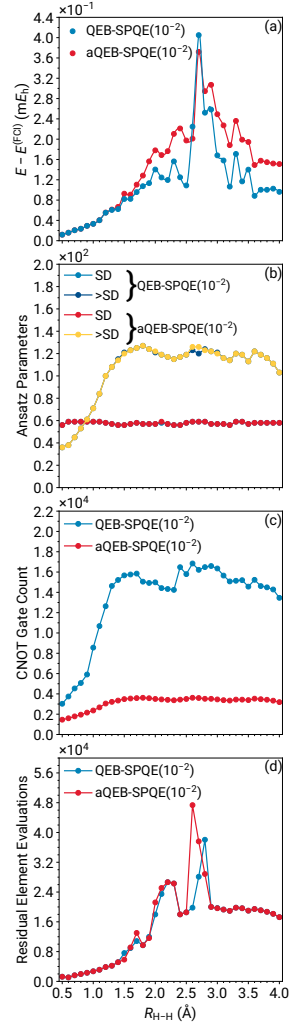


Figure S7: Errors relative to FCI [(a)], ansatz parameters [(b)], CNOT gate counts [(c)], and residual element evaluations [(d)] characterizing the QEB- and aQEB-SPQE(10^{-2}) simulations of the symmetric dissociation of the linear H_6 /STO-6G system. The “SD” and “>SD” symbols denote single or double (SD) or higher (>SD) excitation operators.

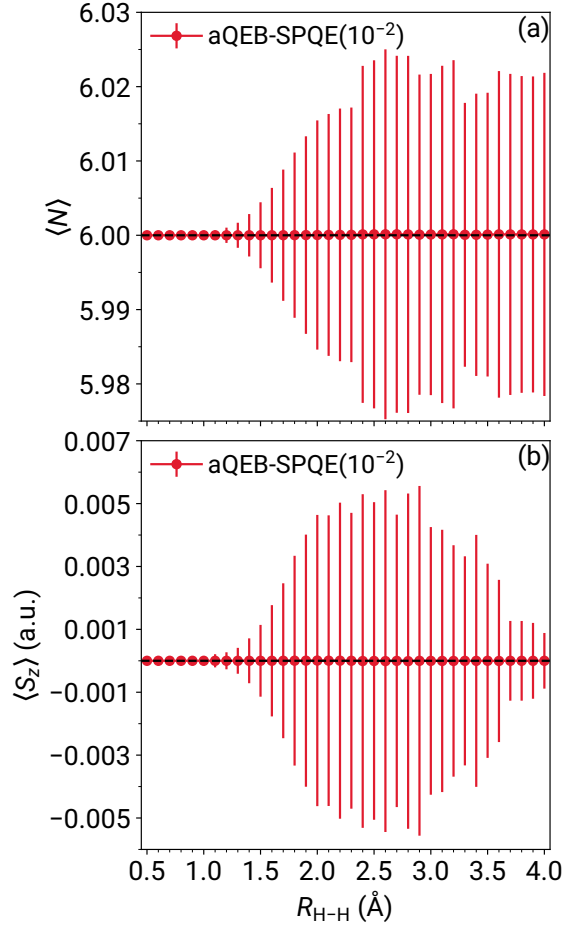


Figure S8: Expectation values of (a) the particle number N and (b) the projection of the total spin on the z axis S_z operators characterizing the aQEB-SPQE(10^{-2}) simulations of the symmetric dissociation of the linear $\text{H}_6/\text{STO-6G}$ system. The vertical lines denote standard deviations, computed as $\sigma_A = \sqrt{\langle A^2 \rangle - \langle A \rangle^2}$. The horizontal dashed lines denote the corresponding eigenvalues for the ground electronic state of the $\text{H}_6/\text{STO-6G}$ linear chain.

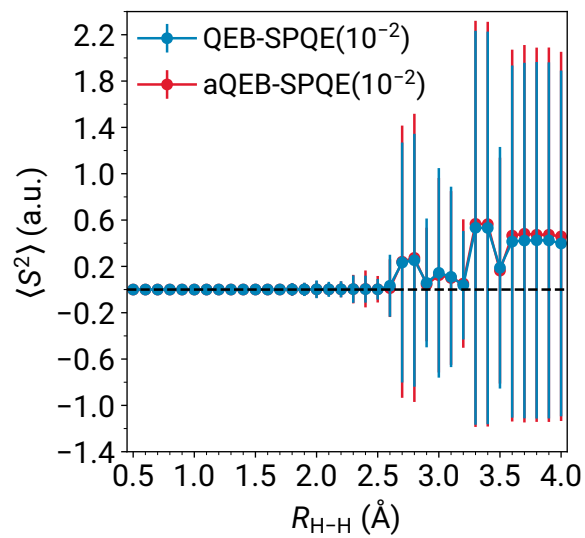


Figure S9: Expectation values of the total spin squared S^2 operator characterizing the QEB- and aQEB-SPQE(10^{-2}) simulations of the symmetric dissociation of the linear $\text{H}_6/\text{STO-6G}$ system. The vertical lines denote standard deviations, computed as $\sigma_A = \sqrt{\langle A^2 \rangle - \langle A \rangle^2}$. The horizontal dashed line denotes the corresponding eigenvalue for the ground electronic state of the $\text{H}_6/\text{STO-6G}$ linear chain.

S2.2 aFEB-SPQE vs aQEB-SPQE

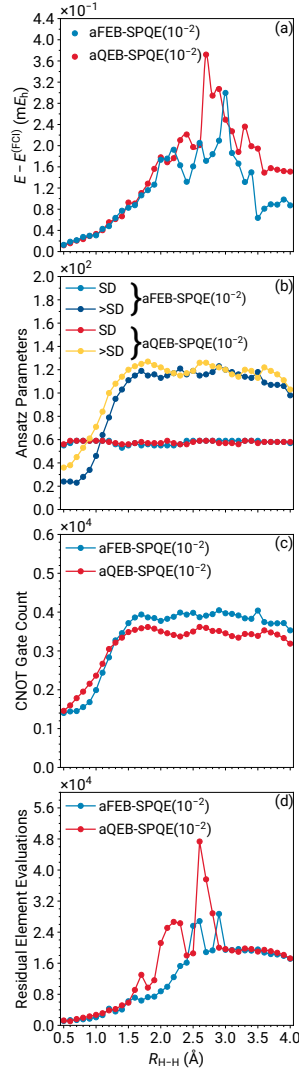


Figure S10: Errors relative to FCI [(a)], ansatz parameters [(b)], CNOT gate counts [(c)], and residual element evaluations [(d)] characterizing the aFEB- and aQEB-SPQE(10^{-2}) simulations of the symmetric dissociation of the linear H₆/STO-6G system. The “SD” and “>SD” symbols denote single or double (SD) or higher (>SD) excitation operators.

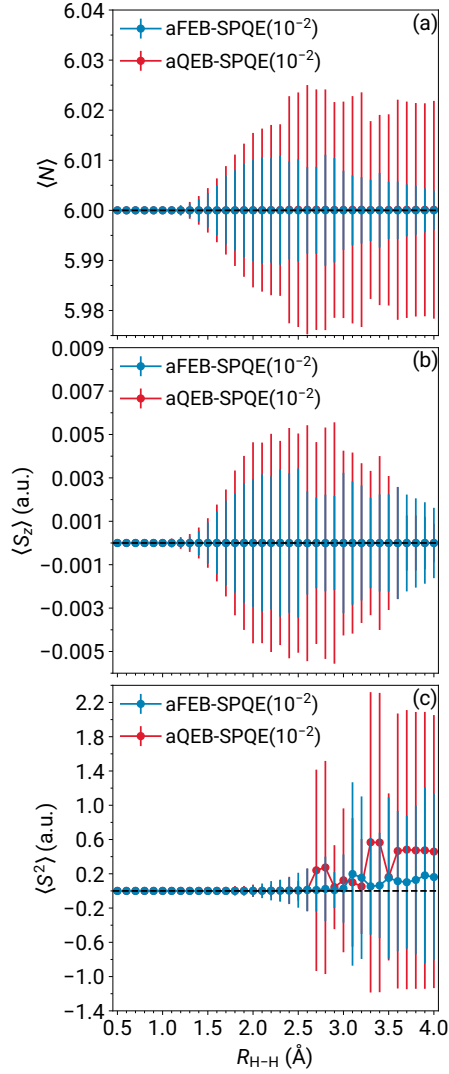


Figure S11: Expectation values of (a) the particle number N , (b) the projection of the total spin on the z axis S_z , and (c) the total spin squared S^2 operators characterizing the aFEB- and aQEB-SPQE(10^{-2}) simulations of the symmetric dissociation of the linear H_6 /STO-6G system. The vertical lines denote standard deviations, computed as $\sigma_A = \sqrt{\langle A^2 \rangle - \langle A \rangle^2}$. The horizontal dashed lines denote the corresponding eigenvalues for the ground electronic state of the H_6 /STO-6G linear chain.